# Signatures of unconventional pairing in near-vortex electronic structure of LiFeAs

Kyungmin Lee,[1] Mark H. Fischer,[1] and Eun-Ah Kim[1]

[1] *Department of Physics, Cornell University, Ithaca, New York 14853, USA*

(Dated: September 6, 2012)

A major question in Fe-based superconductors remains the structure of the pairing, in particular whether it is of unconventional nature. The electronic structure near vortices can serve as a platform for phase-sensitive measurements to answer this question. By solving Bogoliubov-de Gennes equations for LiFeAs, we calculate the energy-dependent local electronic structure near a vortex for different nodeless gap-structure possibilities. At low energies, the local density of states (LDOS) around a vortex is determined by the normal-state electronic structure. However, at energies closer to the gap value, the LDOS can distinguish an anisotropic from a conventional isotropic $s$-wave gap. We show within our self-consistent calculation that in addition, the local gap profile differs between a conventional and an unconventional pairing. We explain this through admixing of a secondary order parameter within Ginzburg-Landau theory. In-field scanning tunneling spectroscopy near vortices can therefore be used as a real-space probe of the gap structure.

PACS numbers: ...

## I. INTRODUCTION

The gap structure in the iron-based superconductors and its possible unconventional nature is still a key issue in the field four years after their discovery. In most compounds of the family, the pairing is believed to be of the so-called $s^{\pm}$ type, for which the order parameter changes sign between the electron-like and the hole-like Fermi surfaces.[1] However, a major difficulty in distinguishing such an unconventional pairing state from a trivial $s$-wave gap is that both states are nodeless and transform trivially under all the symmetry operations of the material's point group. As the experimental probes that are usually used to distinguish various gap structures, such as phase-sensitive probes, are not Fermi pocket specific, an unambiguous evidence of the unconventional $s^{\pm}$ pairing remains evasive.

One route to accessing phase information using a phase insensitive probe would be through vortex bound states, as a vortex introduces a spatial texture to the superconducting order parameter. Advancements in in-field scanning tunneling spectroscopy (STS) enables study of vortex bound states. Indeed, a recent scanning tunneling spectroscopy experiment on LiFeAs under magnetic field has shown intriguing energy dependence in the spatial distribution of local density of states (LDOS) near a vortex.[2] At zero bias, the LDOS shows a four-fold star shape with high-intensity 'rays' along the Fe-As direction, and with increasing energy it exhibits 'splitting of the rays'. The most striking features emerge at energies $E \approx \Delta/2$ as hot spots, at the intersections of two rays.

Motivated by these observations, we present a study of the electronic structure and signature of unconventional pairing near a vortex, within the Bogoliubov-de Gennes (BdG) framework. By imposing a gap structure and solving the BdG Hamiltonian, we show that the isotropic $s$-wave and $s^{\pm}$-wave pairing result in different spatial distributions of the LDOS at energies approaching the gap value. In particular, we find $s^{\pm}$-wave pairing to yield observed hot spots.

For a more direct evidence of unconventional $s^{\pm}$-wave pairing, we propose detecting spatial distribution of the gap around a vortex, based on our self-consistent solutions to the BdG equations. In a conventional isotropic $s$-wave superconductor, a vortex introduces a singular point in space around which the phase of the order parameter winds. In addition, the gap amplitude is completely suppressed at the core of the vortex, but smoothly and isotropically recovers away from the core. However, in an unconventional superconductor, a vortex can also induce a secondary order parameter in its vicinity.[3–9]. This is possible since a symmetry distinction between, for instance, a gap with $s^{\pm} \sim \cos k_x \cos k_y$ and $d_{xy} \sim \sin k_x \sin k_y$ structure is only meaningful in a translationally invariant system. Due to the induced secondary order parameter (which diminishes far from the vortex), the gap recovery should show a strong angular dependence. Detection of such anisotropy will be an unambiguous evidence of unconventional pairing.

The rest of the paper consists of the following: In section II, we present our microscopic model. In section III, we describe our methods. In section IV, we present the results of BdG calculations and insight from corresponding Ginzburg-Landau theory. In section V, we summarize the our findings and remark on future directions.

## II. MODEL

We describe LiFeAs in the superconducting state with the (mean-field) BdG Hamiltonian

$$\mathcal{H}^{\mathrm{BdG}} = \sum_{ij} \Psi_i^{\dagger} \begin{pmatrix} -t_{ij} & \Delta_{ij} \\ \Delta_{ij}^{*} & t_{ij}^{*} \end{pmatrix} \Psi_j. \tag{1}$$

Here, $\Psi_i \equiv (c_{i\uparrow}, c_{i\downarrow}^{\dagger})^T$ is a Nambu spinor, and $c_{is}$ ($c_{is}^{\dagger}$) annihilates (creates) an electron at lattice site $i$ with spin $s$. The kinetic part $t_{ij}$ denotes hopping between sites $i$

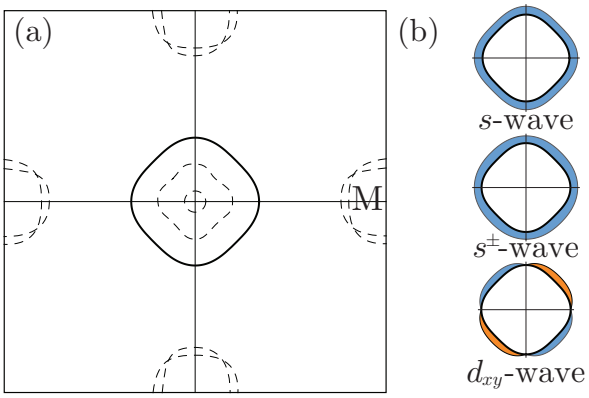


FIG. 1. (a) Fermi surface of LiFeAs with three hole-like pockets around the Γ point and the two electron-like pockets around the $M$ point. In this work, we focus on the $\gamma$ band whose Fermi surface is shown as a bold line. (b) Sketch of the three gap functions with $s$-, $s^{\pm}$-, and $d_{xy}$-wave momentum structure around the $\gamma$-band Fermi surface.

and $j$, and $\Delta_{ij}$ are the (bond) gap functions. To solve $\mathcal{H}^{\mathrm{BdG}}$ self-consistently, the gap functions have to satisfy

$$\Delta_{ij} = \frac{1}{2} V_{ij} \left\langle c_{i\downarrow} c_{j\uparrow} + c_{j\downarrow} c_{i\uparrow} \right\rangle , \tag{2}$$

where $V_{ij} < 0$ is the attractive interaction between sites $i$ and $j$ in the singlet channel and $\langle\cdot\rangle$ denotes the thermal expectation value. Restricting the interaction $V_{ij}$ to a specific form constrains the momentum structure of the gap function, since $\Delta_{ij} \neq 0$ only if $V_{ij} \neq 0$. In the uniform case, on-site attraction $V_{ij} = U\delta_{ij}$ leads to spin-singlet $s$-wave gap

$$\Delta_s(\mathbf{k}) = \Delta_s^0, \tag{3a}$$

while next-nearest-neighbor (NNN) attraction $V_{ij} = V'\delta_{\langle\langle i,j\rangle\rangle}$ allows for the singlet gap functions of $s^{\pm}$

$$\Delta_{s^{\pm}}(\mathbf{k}) = 4\Delta_{s^{\pm}}^0 \cos k_x \cos k_y \tag{3b}$$

and $d_{xy}$ form

$$\Delta_{d_{xy}}(\mathbf{k}) = 4\Delta_{d_{xy}}^0 \sin k_x \sin k_y \tag{3c}$$

in the reciprocal space.

In this paper, we focus on a single band: the so-called $\gamma$ band. The Fermi surface of the $\gamma$ band is shown in Fig. 1(a) (solid line) along with four other bands (dashed lines) crossing the Fermi level in LiFeAs.[10–13] This choice is motivated by the $\gamma$ band's smaller gap value.[11,14] Moreover, this band mainly stems from the (in-plane) $d_{xy}$ orbitals, and hence shows little $k_z$ dependence.[12] Our choice of $t_{ij}$, guided by the experimental observations on the $\gamma$ pocket,[11,14,15] is $t = -0.25$eV for nearest-neighbor hopping, $t' = 0.082$eV for next-nearest-neighbor hopping, and $t_{ii} = \mu = 0.57$eV for the chemical potential. Notice the highly anisotropic (square-like) Fermi surface of this band shown in Fig. 1(a). At low energies, these flat (quasi-one-dimensional) parts of the electronic structure dominate over the small anisotropy of the $s^{\pm}$ gap [see Fig. 1(b)] in determining the near-vortex LDOS.

We introduce vortices into the system through two approaches. First, we fix the non-zero gap functions for both on-site $s$-wave pairing and NNN $s^{\pm}$-wave pairing by hand to

$$\Delta_{ij} = \Delta^0 \tanh(|\mathbf{r}_{ij}|/\xi) e^{i\theta_{ij}}, \tag{4}$$

where the vector $\mathbf{r}_{ij}$ points to the midpoint of sites $i$ and $j$, and $\theta_{ij}$ is its azimuthal angle measured from the Fe-Fe direction. This therefore corresponds to a single vortex suppressing the gap at the core located at the origin and with phase winding around it. Second, we also perform self-consistent calculations, where we induce the formation of vortices by applying a magnetic field $H\hat{\mathbf{z}}$ on the system. Assuming minimal coupling between an electron and the field, the hopping between sites $i$ and $j$ acquires a Peierls phase

$$t_{ij} \longrightarrow t_{ij} e^{i\varphi(\mathbf{r}_i, \mathbf{r}_j)} \tag{5}$$

with

$$\varphi(\mathbf{r}_i, \mathbf{r}_j) \equiv -\frac{\pi}{\Phi_0} \int_{\mathbf{r}_j}^{\mathbf{r}_i} \mathbf{A}(\mathbf{r}) \cdot d\mathbf{r}, \tag{6}$$

where $\Phi_0 = h/2e$ is the magnetic fluxoid and $\mathbf{r}_i$ is the vector pointing to site $i$. We assume uniform magnetic field $H$ and write the vector potential in the Landau gauge $\mathbf{A}(\mathbf{r}) = -Hy\hat{\mathbf{x}}$.

From the self-consistent solution $\Delta_{ij}$, we can define local gap order parameters of different symmetries. For an on-site interaction, the local $s$-wave order parameter is defined as

$$\Delta_s(\mathbf{r}) = \Delta_{\mathbf{r},\mathbf{r}}. \tag{7a}$$

Note that from here on, we use $\mathbf{r}$ without any site index to denote both a lattice site and the corresponding vector in units of the lattice constant $a_0$. With NNN interaction, we define local order parameters of $s^{\pm}$

$$\Delta_{s^{\pm}}(\mathbf{r}) = [\widetilde{\Delta}_{\mathbf{r}+(1,1),\mathbf{r}} + \widetilde{\Delta}_{\mathbf{r}+(1,-1),\mathbf{r}} + \widetilde{\Delta}_{\mathbf{r}+(-1,-1),\mathbf{r}} + \widetilde{\Delta}_{\mathbf{r}+(-1,1),\mathbf{r}}]/4 \tag{7b}$$

and $d_{xy}$ form

$$\Delta_{d_{xy}}(\mathbf{r}) = [\widetilde{\Delta}_{\mathbf{r}+(1,1),\mathbf{r}} - \widetilde{\Delta}_{\mathbf{r}+(1,-1),\mathbf{r}} + \widetilde{\Delta}_{\mathbf{r}+(-1,-1),\mathbf{r}} - \widetilde{\Delta}_{\mathbf{r}+(-1,1),\mathbf{r}}]/4, \tag{7c}$$

where

$$\widetilde{\Delta}_{\mathbf{r}\mathbf{r}'} \equiv \Delta_{\mathbf{r}\mathbf{r}'} e^{-i\varphi(\mathbf{r},\mathbf{r}')}, \tag{8}$$

ensures that order parameters of different symmetries do not mix under magnetic translations. Note that for the uniform case, $\Delta_s(\mathbf{r}) = \Delta_s^0$, $\Delta_{s^{\pm}}(\mathbf{r}) = \Delta_{s^{\pm}}^0$ and $\Delta_{d_{xy}}(\mathbf{r}) = \Delta_{d_{xy}}^0$ of Eqs. (3a)-(3c).

## III. METHOD

In this section, we elaborate on our two approaches to solve the BdG equations and obtain the local density of states near a vortex. For both, diagonalizing the Hamiltonian $\mathcal{H}^{\mathrm{BdG}}$ in Eq. (1) for a system of size $(N_x, N_y)$ is computationally the most expensive part.

### A. Non-Self-Consistent Approach

For the non-self-consistent calculation, we impose a gap function in the form given by Eq. (4) and find the low lying eigenvalues and eigenstates of $\mathcal{H}^{\mathrm{BdG}}$ using the Lanczos algorithm. We suppress the low energy states from forming at the boundary by applying a large potential to the boundary sites. The LDOS can be calculated from the eigenvalues $E^n$ and eigenstates $[u^n(\mathbf{r}), v^n(\mathbf{r})]$ as

$$N(\mathbf{r}, E) \propto \sum_n |u^n(\mathbf{r})|^2 \delta(E - E^n) + |v^n(\mathbf{r})|^2 \delta(E + E^n). \tag{9}$$

Since we are not interested in the absolute value of the LDOS but rather in the spatial profile at a given energy, we normalize the LDOS such that for a given energy $E$, the maximum value of $N(\mathbf{r}, E)$ is unity.

### B. Self-Consistent Approach

For the self-consistent calculation, we assume some initial gap functions and use the eigenvalues and eigenvectors of Eq. (1) to calculate the gap functions given by Eq. (2). We proceed iteratively until self-consistency is achieved. In diagonalizing $\mathcal{H}^{\mathrm{BdG}}$, we can no longer make use of the crystal momentum basis to simplify the problem since the Peierls phase factor prevents the kinetic part of the Hamiltonian from commuting with the ordinary lattice translation operator $T_{\mathbf{R}}$. However, the kinetic part commutes with the magnetic translation operator

$$\hat{T}_{\mathbf{R}} \equiv e^{-i\frac{\pi}{\Phi_0}\mathbf{A}(\mathbf{R})\cdot\mathbf{r}} T_{\mathbf{R}}. \tag{10}$$

for a magnetic lattice vector $\mathbf{R}$ whose unit cell contains two magnetic fluxoids.

The pairing term in general does not commute with $\hat{T}_{\mathbf{R}}$. Nevertheless, when vortices form a lattice, $\hat{T}_{\mathbf{R}}$ commutes with the pairing term if $\mathbf{R}$ is a vector of a vortex sublattice containing every other vortex. Since we focus on the electronic structure near a single vortex, we expect the shape of the vortex lattice to have little effect on our results. Therefore, we make an arbitrary choice for its primitive vectors to be $L_x\hat{\mathbf{x}}$ and $L_y\hat{\mathbf{y}}$, such that $\mathbf{R}$ forms a rectangular lattice $\mathbf{R} = (m_x L_x, m_y L_y)$, where $m_\alpha = 0 \cdots M_\alpha - 1$ and $M_\alpha \equiv N_\alpha / L_\alpha$.[16] Note that periodic boundary conditions in the Landau gauge $\mathbf{A}(\mathbf{r}) = -Hy\hat{\mathbf{x}}$ requires the total magnetic flux through the system to be an integer multiple of $2\Phi_0 N_x$. In addition, one magnetic unit cell contains a magnetic flux of $2\Phi_0$, i.e. $H = 2\Phi_0 / L_x L_y$. We satisfy these two requirements by choosing $M_x = L_y, M_y = L_x$.

Working with the magnetic Bloch states

$$\Psi_{\mathbf{k}}(\mathbf{r}) = \sum_{\mathbf{R}} e^{-i\mathbf{k}\cdot\mathbf{R}}\, \hat{T}_{\mathbf{R}} \Psi(\mathbf{r}) \hat{T}_{\mathbf{R}}^{-1} \tag{11}$$

allows us to block diagonalize the Hamiltonian

$$\mathcal{H}^{BdG} = \frac{1}{M_x M_y} \sum_{\mathbf{k}} \sum_{\mathbf{r},\mathbf{r}'} \Psi_{\mathbf{k}}^\dagger(\mathbf{r}) H_{\mathbf{k}}(\mathbf{r}, \mathbf{r}') \Psi_{\mathbf{k}}(\mathbf{r}'). \tag{12}$$

The indices $\mathbf{k}$ and $\mathbf{r}$ are from here on defined in the magnetic Brillouin zone and magnetic unit cell, respectively, i.e.,

$$\mathbf{k} = \left(2\pi \frac{m_x}{L_x M_x}, 2\pi \frac{m_y}{L_y M_y}\right) \quad m_\alpha = 0 \cdots M_\alpha - 1 \tag{13a}$$

$$\mathbf{r} = (\ell_x, \ell_y) \quad \ell_\alpha = 0 \cdots L_\alpha - 1. \tag{13b}$$

By diagonalizing the matrices $H_{\mathbf{k}}$ of dimension $2L_x L_y \times 2L_x L_y$, we can compute the eigenstates and eigenenergies of $\mathcal{H}^{BdG}$. These are then used to calculate $\Delta_{ij}$ with Eq. (2) closing the self-consistency cycle.

We use the self-consistent solution $\Delta_{ij}$ to calculate the local order parameters of specific symmetries as defined in Eqs. (7a)-(7c) and also the LDOS of the electronic degrees of freedom, as defined in Eq. (9).

## IV. RESULTS

### A. Non-Self-Consistent Approach

Figure 2 shows the near-vortex LDOS calculated by diagonalizing $\mathcal{H}^{\mathrm{BdG}}$ in Eq. (1) with fixed gap functions as given by Eq. (4) on a system of dimension $(N_x, N_y) = (301, 301)$. We choose realistic values of the parameters for the coherence length $\xi = 16.4 a_0$[17,18] and gap values $\Delta_s^0 = 3\mathrm{meV}$ for on-site pairing and $\Delta_{s^\pm}^0 = 1.5\mathrm{meV}$ for NNN pairing.[11,14,15]

We can interpret the vortex bound states in this non-self-consistent BdG calculation as bound states in a trap potential given by Eq. (4), where only states around the normal state Fermi surface constitute the bound states. There are then two sources of anisotropy: anisotropic, quasi-one-dimensional low-energy properties of the normal state, and an anisotropic gap, both defined in the momentum space in the translationally-invariant system.

We first focus on the low energy LDOS [Figs. 2(a) and (b)], where the normal-state properties dominate. For both types of pairing, the bound state is located at the center of the trap. Since the Bloch states making up this bound state have two main velocities due to the quasi-one-dimensional parts of the Fermi surface, the bound state only extends in these two directions out of the trap,

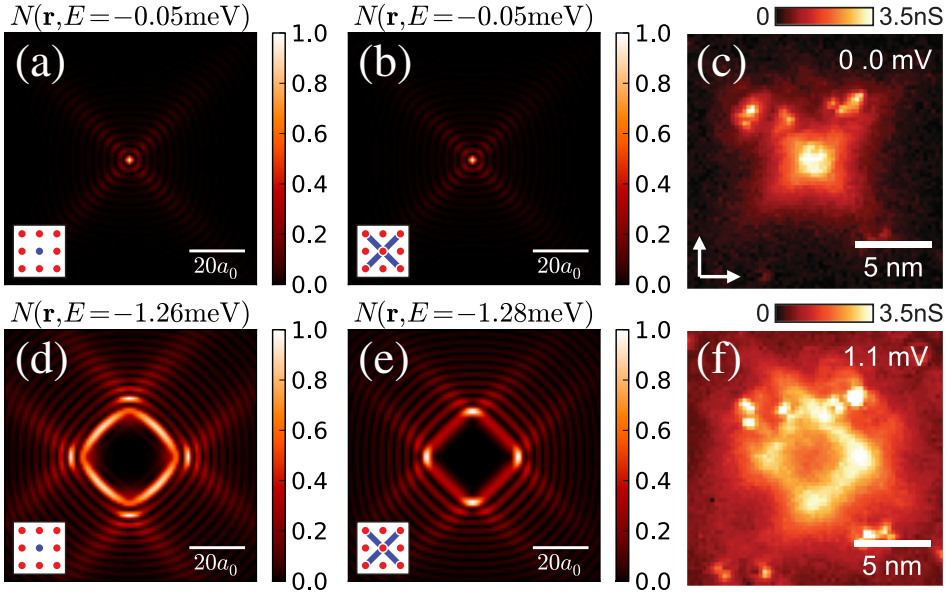


FIG. 2. Local density of states near a vortex for non-self-consistent calculation with the gap function given by Eq. (4). The value $N(\mathbf{r}, E)$ has been normalized such that the maximum value in each map is unity. (a) is the LDOS at the lowest bound state energy with on-site pairing with $\Delta^0 = 3$meV, and (d) is at higher energy. (b) and (e) are with NNN pairing with $\Delta^0 = 1.5$meV. (c) and (f) are the near-vortex LDOS maps observed by Hanaguri *et al.*[2].

resulting in the rays in Fig. 2(a) and (b). The gap is suppressed near the vortex center, and its anisotropy is of little importance.

At higher energies, on the other hand, the bound state is located away from the vortex core. The quasi-one-dimensionality of the Fermi surface allows for localization in one direction and extended parts in the other direction. This leads to a square-like inner ring in the LDOS for both cases [Figs. 2(c) and (d)]. The difference, however, results from the anisotropy of the gap function. While the isotropic $s$-wave gap is analogous to a potential that is independent of the momentum, the anisotropic gap is a trap for which different states around the Fermi surface experience different potentials depending on their momenta. With the gap function of $s^{\pm}$ form, the quasi-one-dimensional portion of the Fermi surface experiences a stronger trap potential, leading to a suppression of its contribution to the bound-state wave function. As a result, the bound state exhibits pronounced isolated segments, 'hot spots', within the inner ring that point in the Fe-Fe direction, as shown in Fig. 2(d).

### B. Self-Consistent Approach

Figure 3 shows the results from the self-consistent calculation. We compare two pairing interactions – on-site attraction $U = -0.35$eV, and NNN attraction $V' = -0.3$eV – for a system with magnetic unit cell of dimensions $(L_x, L_y) = (19, 38)$. This corresponds to a full lattice size of $(N_x, N_y) = (38 \times 19, 19 \times 38)$. In zero field,

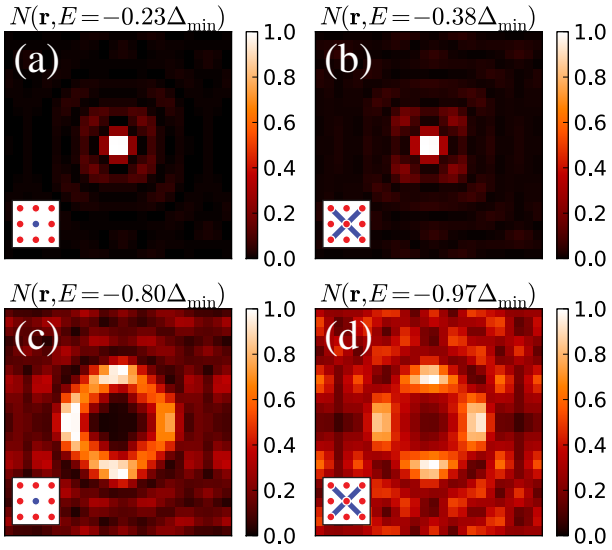


FIG. 3. Local density of states near a vortex for self-consistent calculation. Here again, $N(\mathbf{r}, E)$ is normalized. (a) is the LDOS at the lowest bound state energy with on-site attraction $U = -$eV, and (c) is at higher energy. (b) and (d) are with NNN attraction $V' = -0.3$eV.

the two cases lead to a uniform superconducting gap of $\Delta_s^0 = 27$meV and $\Delta_{s^{\pm}}^0 = 10$meV, respectively. We have chosen $U$ and $V'$ such that the coherence length $\xi \propto \Delta^{-1}$ is small compared to the inter-vortex spacing. This allows us to focus on a nearly isolated vortex within the

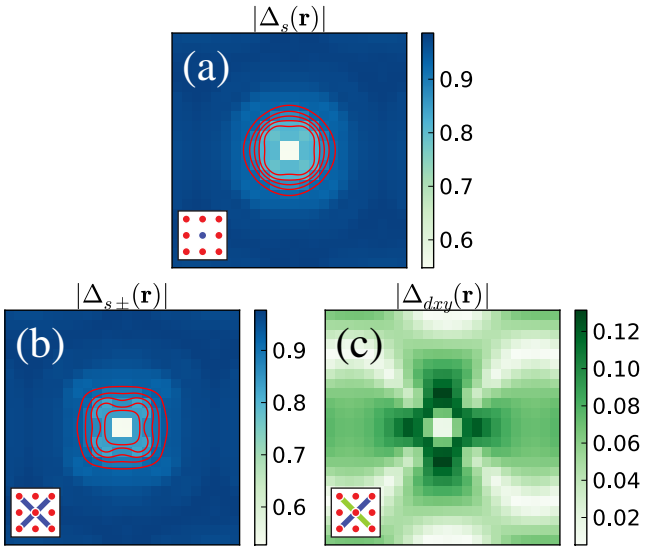


FIG. 4. Spatial distribution of different symmetry components of order parameters. (a) $\Delta_s(\mathbf{r})$ for on-site attraction $U = -0.35$eV. (b) $\Delta_{s\pm}(\mathbf{r})$ and (c) $\Delta_{d_{xy}}(\mathbf{r})$ for NNN pairing $V' = -0.3$eV. The values have been normalized by the value of the dominant order parameter in the absence of magnetic field for each case: $\Delta_s^0$ for (a), and $\Delta_{s\pm}^0$ for (b), (c). The contours in red indicate points at which the amplitude of the order parameter is 0.825 for the innermost, and 0.925 for the outermost contours, with equal intervals between the contours in between. Note that the color-scale for $\Delta_{d_{xy}}(\mathbf{r})$ much smaller than for $\Delta_s(\mathbf{r})$.

computationally feasible size of the magnetic unit cell. Although the resulting gap values are an order of magnitude larger than what is known experimentally, this should not affect the validity of the results in a qualitative manner. Both at low energy and at higher energy close to the gap value, we observe features that qualitatively agree with the results obtained in the previous section.

The self-consistent calculation also allows us to study the local order parameters of a given structure near a vortex. Unlike for the on-site attraction, where $\Delta_s(\mathbf{r})$ is the only allowed gap function, order parameters of different symmetries can mix near a vortex for NNN attraction. A near-vortex map of $\Delta_s(\mathbf{r})$ for on-site pairing shown in Fig. 4(a) indeed shows isotropic healing of the order parameter away from the vortex core. On the other hand, for the NNN attraction which leads to uniform $s^{\pm}$-wave pairing in zero-field, the secondary order parameter $\Delta_{d_{xy}}(\mathbf{r})$ is induced near the vortex. Coupling between this secondary order parameter and the primary $\Delta_{s^{\pm}}(\mathbf{r})$ leads to strong angular variation of both components as can be seen in Figs. 4(b) and (c).

To gain further insight into the admixing of a secondary order parameter near a vortex for the anisotropic pairing, we analyze the Ginzburg-Landau free-energy density. While an on-site attraction only allows for an isotropic $s$-wave component, the NNN pairing allows for both $s$- and $d$-wave components. Hence, the symmetry-based free-energy density corresponding to the NNN-anisotropic-pairing case is

$$\begin{aligned} f =&\alpha_s|s|^2 + \alpha_d|d|^2 + \beta_1|s|^4 + \beta_2|d|^4 + \beta_3|s|^2|d|^2 \\ &+ \beta_4(s^{*2}d^2 + \text{c.c.}) + \gamma_s|\vec{D}s|^2 + \gamma_d|\vec{D}d|^2 \\ &+ \gamma_\nu(D_x s D_y d^* + D_y s D_x d^* + \text{c.c.}), \end{aligned} \tag{14}$$

where $s$ and $d$ are shorthands for $s(\mathbf{r})$ and $d(\mathbf{r})$, the order parameter fields for the $s^{\pm}$ and $d_{xy}$ gaps, respectively, and $D_i = \partial_i - ieA_i$ is the covariant derivative. The fields $s(\mathbf{r})$ and $d(\mathbf{r})$ can be thought of as $\Delta_{s/s^{\pm}}(\mathbf{r})$ and $\Delta_{d_{xy}}(\mathbf{r})$ after coarse graining. This type of admixing near a vortex has previously been studied in the context of cuprates.[3–9][19] As the large halo around vortices in cuprates[20] hindered the observation of this admixing, LiFeAs presents an opportunity for this observation.

The spatial variation of the secondary component $d_{xy}$ in Fig. 4(c) is largely due to the derivative coupling, the term proportional to $\gamma_\nu$ in Eq. (14). For $|s| \gg |d|$ and $|\vec{D}s| \gg |\vec{D}d|$ the spatial structure of the $d_{xy}$ component is determined largely by the structure of the $s$-wave component. Minimizing Eq. (14) with respect to $d(\mathbf{r})$ and keeping only terms up to linear order in $d(\mathbf{r})$, we find

$$-\gamma_d\vec{D}^2 d + \alpha_d d + \beta_3|s|^2 d + \beta_4 s^2 d^* = \gamma_\nu(D_x D_y + D_y D_x)s. \tag{15}$$

Hence, the curvature in the leading $s$-wave component will induce the secondary ($d_{xy}$) component. Now consider a single isolated vortex. As $s(\mathbf{r})$ is recovered at the length scale of the coherence length $\xi$ away from the core of the vortex, we expect a large $d(\mathbf{r})$ due to coupling to the large curvature of $s(\mathbf{r})$ at this distance. Since $\xi = \hbar v_F/\pi\Delta \sim 3.0a_0$ for the uniform gap value with $V' = -0.3$eV, this is in agreement with the positions of the maxima of $d(\mathbf{r})$ in Fig. 4(c) as a function of $|\mathbf{r}|$ setting the vortex core at the origin. We can also explain the angular variation and the form of the anisotropy of $d(\mathbf{r})$ in this framework. If we assume $s(\mathbf{r}) = f(r)e^{i\theta}$ with a slowly changing $f(r)$ and the azimuthal angle $\theta$ measured from the Fe-Fe direction, we find from Eq. (15)

$$d(\mathbf{r}) \sim \partial_x\partial_y s(\mathbf{r}) \sim e^{-i\theta}(1 + 3e^{4i\theta}), \tag{16}$$

ignoring the phase due to the magnetic field. The structure of the derivative hence gives rise to a four-fold anisotropy, which explains the fact that $|d(\mathbf{r})|$ is maximum in the Fe-Fe direction, while it is suppressed along the 45° direction. Coupling to $d(\mathbf{r})$ gives then in turn cause for the four-fold anisotropy in $s(\mathbf{r})$.

## V. CONCLUSION

We have contrasted effects of anisotropic $s^{\pm}$-wave (NNN pairing) and isotropic $s$-wave (on-site pairing) on

the near-vortex local density of states in LiFeAs, by solving Bogoliubov-de Gennes equations both non-self-consistently and self-consistently. We find qualitative changes in the geometric distribution of the density of states as a function of energy. At low energies, the anisotropy of the vortex bound state, and hence the LDOS, are determined by the normal-state low energy electronic structure, independently of the gap structure. The different pairing structures, however, lead to qualitatively different LDOS distribution at higher energies: While the isotropic $s$-wave shows a square-like feature of roughly equal intensity, four 'hot spots' develop in the case of an (anisotropic) $s^{\pm}$-wave gap. Indeed, our results for the latter case qualitatively agree with recent experiments by Hanaguri *et al.*[2].

From a self-consistent treatment we further find a difference in the recovery of the order parameter away from the vortex core: a pronounced angular dependence of the $s^{\pm}$-wave gap compared to isotropic behavior for the $s$-wave gap. Employing a Ginzburg-Landau analysis, we explain this difference through admixing of a secondary order parameter supported by the NNN interaction. Detection of the anisotropy or even the secondary order parameter would be a strong proof of the unconventional nature of the pairing.

Here we focused on the $\gamma$ band with interest in low energy properties, as this is the band with the smallest gap.[11,14] Hence for features at energies much less than the gap energy at the electron pockets, we expect our calculation to capture salient features of in-field STS experiments. The comparison between the calculated LDOS and the results in Ref. 2 confirms this conjecture.

In closing we note that our calculation captures Friedel-like oscillations, frequently referred to as quasiparticle interference (QPI), due to vortices. QPI in the presence of vortices was successfully used to access phase information with STS in cuprates.[21] Recent in-field QPI experiments on FeSe have been interpreted to be consistent with an $s^{\pm}$ scenario when a vortex is treated as a magnetic scatterer for BdG quasiparticles.[22] However, a vortex is at once a point of gap suppression, a point with magnetic flux and a point around which the order-parameter phase winds. While we treated vortices faithfully in this work, we could not investigate effects of inter-pocket sign change as we only considered one pocket. An extension of the present work with the full band structure would be necessary to work out what to expect for different order-parameter possibilities, especially how the phase difference between different pockets affects in-field QPI.

## ACKNOWLEDGMENTS

We are grateful to M. Allan, J. Berlinsky, J.C. Davis, T. Hanaguri, C. Kallin, A.W. Rost, I. Firmo, and Z. Tesanovic for helpful discussions. We acknowledge support from NSF Grant DMR-0955822. MHF and E-AK additionally acknowledge support from NSF Grant DMR-0520404 to the Cornell Center for Materials Research.

[1] P. J. Hirschfeld, M. M. Korshunov, and I. I. Mazin, Rep. Prog. Phys. **74**, 124508 (2011).
[2] T. Hanaguri, K. Kitagawa, K. Matsubayashi, Y. Mazaki, Y. Uwatoko, and H. Takagi, Phys. Rev. B **85**, 214505 (2012).
[3] A. J. Berlinsky, A. L. Fetter, M. Franz, C. Kallin, and P. I. Soininen, Phys. Rev. Lett. **75**, 2200 (1995).
[4] Y. Ren, J.-H. Xu, and C. S. Ting, Phys. Rev. Lett. **74**, 3680 (1995).
[5] J.-H. Xu, Y. Ren, and C. S. Ting, Phys. Rev. B **52**, 7663 (1995).
[6] M. Franz, C. Kallin, P. I. Soininen, A. J. Berlinsky, and A. L. Fetter, Phys. Rev. B **53**, 5795 (1996).
[7] Y. Ren, J.-H. Xu, and C. S. Ting, Phys. Rev. B **53**, 2249 (1996).
[8] J.-H. Xu, Y. Ren, and C.-S. Ting, Phys. Rev. B **53**, R2991 (1996).
[9] J. J. V. Alvarez, C. A. Balseiro, and G. C. Buscaglia, Phys. Rev. B **58**, 11181 (1998).
[10] D. J. Singh, Phys. Rev. B **78**, 094511 (2008).
[11] S. V. Borisenko, V. B. Zabolotnyy, D. V. Evtushinsky, T. K. Kim, I. V. Morozov, A. N. Yaresko, A. A. Kordyuk, G. Behr, A. Vasiliev, R. Follath, and B. Büchner, Phys. Rev. Lett. **105**, 067002 (2010).
[12] T. Hajiri, T. Ito, R. Niwa, M. Matsunami, B. H. Min, Y. S. Kwon, and S. Kimura, Phys. Rev. B **85**, 094509 (2012).
[13] C. Putzke, A. I. Coldea, I. Guillamón, D. Vignolles, A. McCollam, D. LeBoeuf, M. D. Watson, I. I. Mazin, S. Kasahara, T. Terashima, T. Shibauchi, Y. Matsuda, and A. Carrington, Phys. Rev. Lett. **108**, 047002 (2012).
[14] K. Umezawa, Y. Li, H. Miao, K. Nakayama, Z.-H. Liu, P. Richard, T. Sato, J. B. He, D.-M. Wang, G. F. Chen, H. Ding, T. Takahashi, and S.-C. Wang, Phys. Rev. Lett. **108**, 037002 (2012).
[15] M. P. Allan, A. W. Rost, A. P. Mackenzie, Y. Xie, J. C. Davis, K. Kihou, C. H. Lee, A. Iyo, H. Eisaki, and T.-M. Chuang, Science **336**, 563 (2012).
[16] This choice yields an oblique vortex lattice, since there are two vortices in each (rectangular) magnetic unit cell, trying to form a triangular vortex lattice as a self-consistent solution.
[17] B. Lee, S. Khim, J. S. Kim, G. R. Stewart, and K. H. Kim, EPL (Europhysics Letters) **91**, 67002 (2010).
[18] N. Kurita, K. Kitagawa, K. Matsubayashi, A. Kismarahardja, E.-S. Choi, J. S. Brooks, Y. Uwatoko, S. Uji, and T. Terashima, J. Phys. Soc. Jpn. **80**, 013706 (2012).
[19] The microscopic model we consider is related to the one-band model of cuprates through rotation by 45°, the roles played by $s$-wave and $d$-wave order parameters are reversed and our $d$-wave order parameter is of $d_{xy}$ form rather than

$d_{x^2-y^2}$.

[20] J. E. Hoffman, E. W. Hudson, K. M. Lang, V. Madhavan, H. Eisaki, S. Uchida, and J. C. Davis, Science **295**, 466 (2002).

[21] T. Hanaguri, Y. Kohsaka, M. Ono, M. Maltseva, P. Coleman, I. Yamada, M. Azuma, M. Takano, K. Ohishi, and H. Takagi, Science **323**, 923 (2009).

[22] T. Hanaguri, S. Niitaka, K. Kuroki, and H. Takagi, Science **328**, 474 (2010).